Limnol. Oceanogr., 57(5), 2012, 1453–1466

doi:10.4319/lo.2012.57.5.1453

The spectral slope coefficient of chromophoric dissolved organic matter ($S_{275–295}$) as a tracer of terrigenous dissolved organic carbon in river-influenced ocean margins

Cédric G. Fichot,[a,*] and Ronald Benner [a,b]

[a] Marine Science Program, University of South Carolina, Columbia, South Carolina
[b] Department of Biological Sciences and Marine Science Program, University of South Carolina, Columbia, South Carolina

Abstract

The present study demonstrates that the spectral slope coefficient of chromophoric dissolved organic matter (CDOM) between 275 nm and 295 nm ($S_{275–295}$) can be used as a tracer of the percent terrigenous dissolved organic carbon (%tDOC) in river-influenced ocean margins, where rivers exert an important control on carbon dynamics and CO_2 fluxes. Absorption coefficients of CDOM and concentrations of dissolved organic carbon (DOC) and dissolved lignin were measured on a seasonal basis in the Mississippi and Atchafalaya rivers and in surface waters of the northern Gulf of Mexico (NGoM). A strong, linear relationship between lignin concentrations and CDOM absorption coefficients indicated lignin is an important chromophore in this environment. The dual nature of lignin as an important chromophore in CDOM and as a terrigenous component of DOC facilitated development of the tracer. The applicability of the tracer relies on the existence of a strong, nonlinear relationship between $S_{275–295}$ and the DOC-normalized lignin yield in rivers and along the freshwater–marine continuum in the NGoM. Physical mixing and the effects of photodegradation on $S_{275–295}$ and dissolved lignin were largely responsible for maintaining this relationship, suggesting the tracer is applicable to surface waters of most river-influenced ocean margins. The spectral slope coefficient ($S_{275–295}$) provides new capabilities to trace tDOC on synoptic scales of relevance to ocean margins and represents an important tool for improving ocean carbon budgets.

The key processes controlling carbon transformations in ocean margins remain poorly quantified, thereby limiting our understanding of how the coastal ocean affects the ocean carbon cycle and atmospheric CO_2. Ocean margins account for $< 10\%$ of the global ocean surface area but play a disproportionately large role in ocean primary production, carbon remineralization, and carbon burial (Gattuso et al. 1998; Muller-Karger et al. 2005). Yet, estimation of carbon budgets remains a formidable challenge in ocean margins because the complex interplay of biogeochemical and physical processes inherent to these systems results in spatially and temporally variable carbon fluxes. Major questions thus remain as to whether ocean margins are net heterotrophic or autotrophic systems (Smith and Hollibaugh 1993; Gattuso et al. 1998) and as to why some ocean margins are net sources of CO_2 to the atmosphere whereas others are net sinks (Borges et al. 2005; Cai et al. 2006). Such uncertainties in net carbon metabolism and air–sea CO_2 exchange have left ocean margins largely unaccounted for in global carbon budgets.

Rivers exert an important control on carbon dynamics in ocean margins by contributing $\simeq 0.25$ Pg C yr^{-1} of terrigenous dissolved organic carbon (tDOC) to the coastal ocean (Hedges et al. 1997). The fate of tDOC in the ocean and its effects on the net carbon metabolism of ocean margins are strongly dependent on whether tDOC is remineralized on the continental shelf or is transported to the open ocean. Isotopic and biomarker measurements indicate that tDOC represents a very small fraction of the dissolved organic carbon (DOC) pool in the ocean (Druffel et al. 1992; Hedges et al. 1997; Opsahl and Benner 1997), thereby suggesting that major remineralization routes of tDOC exist in ocean margins. Although considerable progress has been made understanding the processes involved in the remineralization of tDOC (Smith and Hollibaugh 1993; Cauwet 2002; Mopper and Kieber 2002), the extreme heterogeneity of river-influenced ocean margins represents a major challenge for providing quantitative estimates of these processes. Quantification of tDOC remineralization in ocean margins is largely restrained by the practicality of current tDOC proxies that rely on complex chemical analyses of biomarkers (e.g., lignin) or isotopic composition (e.g., $\delta^{13}C$). Innovative proxies capable of providing high-resolution estimates of tDOC and assessing regional features are therefore critically needed to improve carbon budgets in the coastal ocean.

The spectral absorption coefficient of chromophoric dissolved organic matter (CDOM), denoted here as $a_g(\lambda)$ where λ is the wavelength, possesses attributes of a practical tracer of tDOC in river-influenced ocean margins. Optical measurements of CDOM are amenable to high-resolution and long-term monitoring using ship-based systems, moorings, and remote sensing (Hoge et al. 1995; Chen and Gardner 2004) and can therefore provide the spatio-temporal coverage necessary for a better understanding of the fate of tDOC in ocean margins. Furthermore, recent advances in the biogeochemistry of lignin have revealed that a strong linear relationship between $a_g(\lambda)$ and dissolved lignin exists in rivers (Spencer et al. 2008; Benner and Kaiser 2011) and in river-influenced ocean margins (Hernes and Benner 2003), which suggests that lignin is an important chromophore of dissolved organic matter (DOM) in these environments. Lignin is also exclusively biosynthesized by vascular plants on land, and is therefore

* Corresponding author: cgfichot@gmail.com

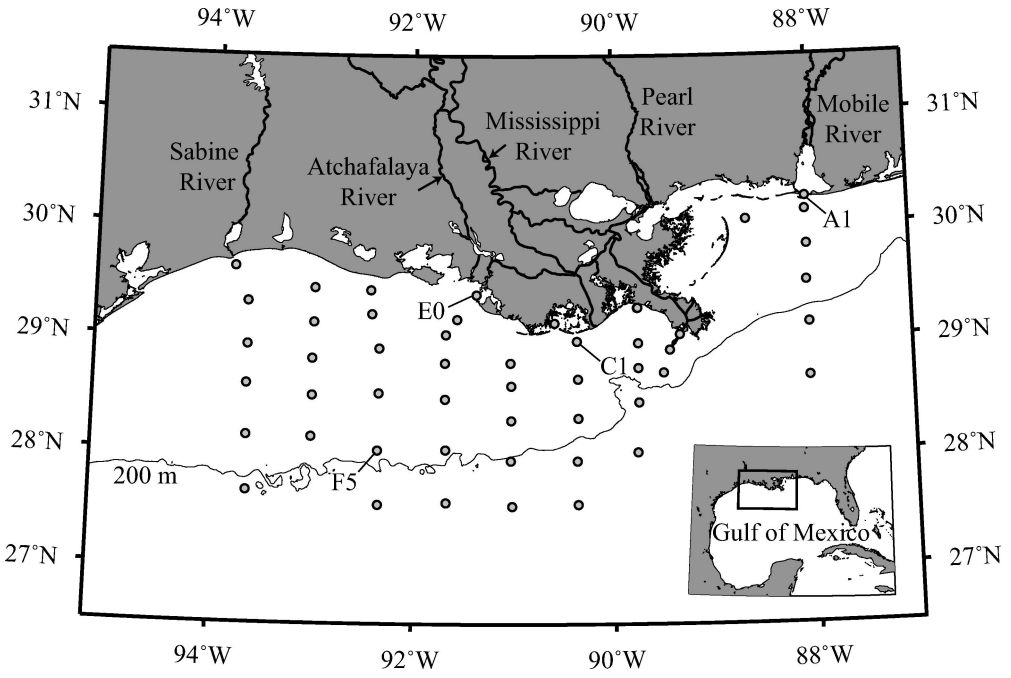

Fig. 1. Study area, sampling stations, and major rivers to the northern Gulf of Mexico. The Mississippi and Atchafalaya rivers contribute about 80% of the freshwater input to this ocean margin. Detailed sampling information is provided in Table 1. The mixing experiment (Fig. 5) was done using surface water from Sta. E0 and F5, collected in November 2009. The DOM amendment and degradation experiments (Table 3) were conducted using surface water from Sta. A1 and C1, collected in March 2010.

a biomarker of terrigenous DOM (Hedges and Mann 1979; Opsahl and Benner 1997). This combination of properties defines lignin as a strictly terrigenous chromophore and suggests it is possible to trace this terrigenous component of DOM using $a_g(\lambda)$ in river-influenced ocean margins.

The CDOM spectral slope coefficient (SSC) in the 275–295-nm spectral range ($S_{275–295}$) could be a robust indicator of the DOC-normalized yield of dissolved lignin (TDLP-C) in river-influenced ocean margins, a quantity that can be exploited to estimate the fraction of DOC of terrigenous origin (Opsahl and Benner 1997). Helms et al. (2008) demonstrated that $S_{275–295}$ is a reliable proxy of CDOM average molecular weight (MW) and also suggested that $S_{275–295}$ is a potential indicator of photobleaching and DOM source in the marine environment. It was later demonstrated that $S_{275–295}$ is also an excellent indicator of the DOC-normalized absorption coefficient of CDOM in the surface waters of two contrasting river-influenced ocean margins, a feature exploited to accurately retrieve DOC concentrations from $a_g(\lambda)$ in these systems (Fichot and Benner 2011). In light of this finding, the strong connection between lignin and $a_g(\lambda)$ suggests $S_{275–295}$ could be useful as a tracer of TDLP-C in river-influenced ocean margins.

In this study, we specifically test this hypothesis and demonstrate that a strong relationship exists between $S_{275–295}$ and TDLP-C in surface waters of the northern Gulf of Mexico (NGoM). We further explore the origin of this relationship and use it to establish a new tracer of tDOC that is applicable on synoptic scales in river-influenced ocean margins. This tracer was developed using in situ measurements of $a_g(\lambda)$, DOC, and lignin concentration acquired on a seasonal basis along a full salinity gradient in the surface waters of the NGoM. The NGoM is one of the largest river-influenced ocean margins in North America and represents an ideal environment for the development of this new approach.

Methods

Study area and sampling overview—Surface-water samples were collected as part of the GulfCarbon project, during five research cruises in the NGoM in January, April, July, and October–November 2009 and March 2010 (Fig. 1 and Table 1). The NGoM is one of the largest river-influenced ocean margins in North America, with the Mississippi River (MR) and the Atchafalaya River (AR) draining 41% of the contiguous USA and accounting for about 80% of the total freshwater input to the NGoM (Rabalais et al. 2002). Two-hundred twenty-two samples were collected for DOC and CDOM analyses, with 104 matching samples for lignin analysis. Samples were collected across a salinity range of 0–37 and are representative of the majority of water types typically encountered in river-influenced ocean margins, from riverine to oligotrophic marine waters. Most samples were collected under well-mixed conditions from Niskin bottles mounted on a rosette with a conductivity–temperature–depth instrument. Samples were collected with a polypropylene bucket deployed from the bow of the ship when a strong vertical salinity gradient was observed in river plumes.

DOC sampling and analysis—Samples were gravity-filtered from Niskin bottles using precombusted glass-fiber (GF/F) filters (0.7-μm pore size) and stored frozen (−20°C)

Table 1. GulfCarbon 2009–2010 sampling information. n is the number of samples collected for DOC and CDOM analyses whereas n_{lignin} is the number of corresponding samples collected for lignin analyses. Ranges and median values of salinity and temperature are for all collected samples (n).

Research cruise	Season	Sampling dates	Number of samples	Salinity	Temperature (°C)
			n (n_{lignin})	Min-max (median)	Min-max (median)
		2009			
GC1	Winter	09 Jan–18 Jan	24 (18)	0–36.45 (32.32)	8.0–22.9 (18.4)
GC2	Spring	20 Apr–30 Apr	50 (23)	0–36.95 (34.20)	15.1–24.6 (22.7)
GC3	Summer	19 Jul–29 Jul	51 (21)	0–36.77 (32.32)	27.5–30.8 (29.7)
GC4	Autumn	29 Oct–07 Nov	47 (22)	0–36.63 (32.70)	16.7–27.4 (23.7)
		2010			
GC5	Winter to spring	11 Mar–20 Mar	50 (20)	0–36.48 (28.32)	10.6–20.3 (17.0)
Total			222 (104)	0–36.95 (32.16)	8.0–30.8 (22.7)

immediately after collection in precombusted borosilicate glass vials. DOC analysis was conducted within a month of collection by high-temperature combustion using a Shimadzu total organic carbon TOC-V analyzer equipped with an autosampler (Benner and Strom 1993). Blanks were negligible and the coefficient of variation between injections of a given sample was typically ± 0.6%. Accuracy and consistency of measured DOC concentrations was checked by analyzing a deep seawater reference standard (University of Miami) every sixth sample.

CDOM sampling and analysis—Samples were gravity-filtered from Niskin bottles using Whatman Polycap Aqueous Solution (AS) cartridges (0.2-μm pore size), collected in precombusted borosilicate glass vials, and stored immediately at 4°C until analysis in the laboratory. For most samples, the absorbance was measured from 250 nm to 800 nm using a Shimadzu ultraviolet (UV)-visible UV-1601 dual-beam spectrophotometer and 10-cm cylindrical quartz cells. For highly absorbing samples, 5-cm cylindrical quartz cells or 1-cm quartz cuvettes were used. An exponential fit of the absorbance spectrum over an optimal spectral range was used to derive an offset value that was subtracted from the absorbance spectrum (Johannessen and Miller 2001; Fichot and Benner 2011). Absorbance corrected for offset was then converted to Napierian absorption coefficient, $a_g(\lambda)$ (m^{-1}). The dependence of $a_g(\lambda)$ on λ is typically described using Eq. 1:

$$a_g(\lambda) = a_g(\lambda_0)e^{-S(\lambda-\lambda_0)} \quad (1)$$

where $\lambda_0 < \lambda$ and S is the spectral slope coefficient in the λ_0–λ-nm spectral range. Spectral slope coefficients were estimated using a linear fit of the log-linearized $a_g(\lambda)$ spectrum over their respective spectral range and are reported here with units of nm^{-1}. Measurements of DOC and $a_g(350)$ were used to calculate DOC-normalized absorption coefficients ($a_g(350)$: DOC), expressed here in units of L mol^{-1} cm^{-1}.

Lignin sampling, extraction, and analysis—Samples were gravity-filtered from Niskin bottles using Whatman Polycap AS cartridges (0.2-μm pore size), collected in 10-liter high-density polyethylene carboys and acidified to pH ≃ 2.5–3 with 5 mol L^{-1} sulfuric acid. Acidified samples were extracted onboard using C-18 cartridges (Varian MegaBond Elut) at a flow rate of 50 mL min^{-1} (Louchouarn et al. 2000), and cartridges were stored at 4°C until elution in 30 mL of high-precision liquid chromatography (HPLC)-grade methanol and stored at −20°C. Lignin was analyzed using the CuO oxidation method of Kaiser and Benner (2012).

Concentrations of lignin phenols were measured as trimethylsilyl derivatives using an Agilent 7890 gas chromatograph equipped with a Varian DB5-MS capillary column and an Agilent 5975 mass selective detector. The concentrations of nine lignin phenols were measured in this study: *p*-hydroxybenzaldehyde (PAL), *p*-hydroxyacetophenone (PON), *p*-hydroxybenzoic acid (PAD), vanillin (VAL), acetovanillone (VON), vanillic acid (VAD), syringaldehyde, acetosyringone, syringic acid. PAL and PAD can be potentially produced from nonlignin sources during CuO oxidation (Benner and Kaiser 2011), but a strong linear relationship ($R^2 \simeq 0.95$) between the sum of *p*-hydroxy phenols (PAL + PAD + PON) and the sum of vanillyl phenols (VAL + VAD + VON), and a strong linear relationship ($R^2 \simeq 0.99$) between PAL or PAD and PON, which is derived from lignin, indicated that PAL and PAD were derived from lignin. The sum of six vanillyl and syringyl lignin phenols ($TDLP_6$), and the sum of nine *p*-hydroxyl, vanillyl, and syringyl lignin phenols ($TDLP_9$) are reported in units of nmol L^{-1}. Corresponding DOC-normalized lignin yields ($TDLP_6$-C and $TDLP_9$-C) are reported in units of %DOC.

Riverine DOM mixing experiment—Surface water from Sta. E0 (riverine) and F5 (marine) were collected during the GC4 cruise (Fig. 1) and combined with different mix-ratios to simulate conservative mixing of riverine DOC into marine waters. The riverine (Salinity = 0, DOC = 600 μmol L^{-1}) and marine (Salinity = 36.6, DOC = 78 μmol L^{-1}) samples were mixed in the following proportions (E0/F5 % vol.): 100/0, 50/50, 10/90, 2.5/97.5, 1.25/98.75, and 0/100, corresponding to salinities of 0, 18.3, 32.9, 35.8, 36.1, and 36.6, respectively. The $TDLP_9$-C values were calculated using mixing ratios and DOC and lignin phenol concentrations measured in the E0 and F5 samples. Theoretical $a_g(\lambda)$ spectra were calculated in the same manner and 'theoretical' values of $S_{275–295}$ were derived. The $a_g(\lambda)$ spectra were also measured for each mixture and 'measured' values of $S_{275–295}$ were calculated.

Photobleaching and lignin photodegradation experiments—Samples for photobleaching experiments were gravity-filtered from Niskin bottles using Whatman Polycap AS cartridges (0.2-μm pore size), collected in cleaned (450°C for 4 h) 500-mL Kimax glass bottles and stored immediately at 4°C. Prior to each experiment, samples were refiltered through a 0.2-μm nylon-membrane filter before dispensing into 5-cm pathlength quartz cells (Spectrocell CM-3050-T). Quadruplicates of each sample were irradiated under controlled illumination conditions and constant temperature (22.5°C) using an Atlas Suntest XPS+ solar simulator (Xenon lamp, 750 W) and a setup similar to the one used by Johannessen and Miller (2001). Long-pass, 295-nm cutoff filters (Schott N-WG295) were used to prevent unnatural radiation from reaching the samples. Irradiations lasted 48 h for most samples, and 72 or 96 h for a few samples. Changes in $a_g(\lambda)$ (λ = 250–800 nm) and $S_{275–295}$ were monitored every 24 h, regardless of total irradiation time. Seventy-five samples were processed during the five cruises. Duplicate experiments were conducted for 6 of the 75 samples.

Changes in $TDLP_9$-C during irradiation were measured using five samples collected during the GC5 cruise. About 250 mL of sample was divided and dispensed into eight quartz cells before irradiation using the same setup as in the photo-beaching experiments (48-h irradiations). After irradiation, the eight subsamples were consolidated into one sample and analyzed for $a_g(\lambda)$ (λ = 250–800 nm), DOC, and lignin, and $TDLP_9$-C and $S_{275–295}$ were calculated. About 250 mL of the original sample was also used in the same analyses in order to provide initial values.

Plankton DOM amendment and microbial degradation experiments—During the GC5 cruise, surface waters from Sta. A1 and C1 (Fig. 1) were gravity-filtered from Niskin bottles using precombusted GF/F filters (0.7-μm pore size) and used onboard in microbial degradation experiments. For both stations, 2 liters of filtered water was divided into two treatments: unamended or amended with $\simeq$ 22 μmol (DOC) L^{-1} of plankton DOM obtained from a diatom bloom (Davis and Benner 2007). For each treatment, triplicates dispensed in cleaned (450°C for 4 h), 125-mL Kimax glass bottles were immediately frozen at −20°C (initial time point), and matching triplicates were incubated onboard in the dark, at ambient seawater temperatures (10–20°C) and under oxic conditions. Incubation times were 12 d for sample A1 and 10 d for sample C1. Samples were frozen at −20°C after incubation. Triplicates were analyzed for DOC and total dissolved amino acids (TDAA) analyses. The TDAA concentrations were measured as *o*-phthaldialdehyde derivatives using an Agilent 1100 HPLC system with a fluorescence detector (Shen et al. 2012). The rest of each sample was filtered through a 0.2-μm nylon-membrane filter and analyzed for CDOM. The triplicates from each treatment and time point were combined prior to filtration and analyzed for CDOM as one sample.

Results

DOM properties in the NGoM—The relationships between DOM properties and salinity indicated a dominant influence of terrigenous inputs from the MR and AR on DOM dynamics (Fig. 2). Values of DOC, $TDLP_9$, $TDLP_9$-C, $a_g(350)$, and $a_g(350)$: DOC were highest in the MR and AR, where they ranged from 232 μmol L^{-1} to 611 μmol L^{-1}, 71 nmol L^{-1} to 491 nmol L^{-1}, 0.22 %DOC to 0.68 %DOC, 3.96 m^{-1} to 17.52 m^{-1}, and 153 L mol^{-1} cm^{-1} to 292 L mol^{-1} cm^{-1}, respectively. These DOM properties decreased from riverine to oligotrophic marine waters, where they reached minimum values of 63 μmol L^{-1} (DOC), 1 nmol L^{-1} ($TDLP_9$), 0.01 %DOC ($TDLP_9$-C), 0.046 m^{-1} (a_g[350]), and 5.8 L mol^{-1} cm^{-1} (a_g[350] : DOC). Coefficients of determination (R^2) associated with seasonal linear regressions of DOM properties on salinity further indicated that 82–94%, 67–90%, 54–92%, 83–94%, and 75–93% of the variability in DOC, $TDLP_9$, $TDLP_9$-C, $a_g(350)$, and $a_g(350)$: DOC, respectively, were related to changes in salinity.

The relationships between DOM properties and salinity also revealed distinct and seasonally variable riverine DOM sources (Fig. 2). Variability in riverine source was evident from seasonal changes and scatter in the relationships between DOC, $TDLP_9$, $TDLP_9$-C, $a_g(350)$, $a_g(350)$: DOC, and salinities < 25. This observation is supported by large differences in these properties between the MR and the AR. The DOC, $TDLP_9$, $TDLP_9$-C, $a_g(350)$, and $a_g(350)$: DOC in the MR averaged (± SD) 296 ± 54 μmol L^{-1}, 135 ± 52 nmol L^{-1}, 0.37 ± 0.10 %DOC, 5.54 ± 1.63 m^{-1}, and 185 ± 30 L mol^{-1} cm^{-1}, respectively, and are lower than in the AR where they averaged 438 ± 106 μmol L^{-1}, 266 ± 147 nmol L^{-1}, 0.48 ± 0.18 %DOC, 10.43 ± 4.19 m^{-1}, and 233 ± 40 L mol^{-1} cm^{-1}, respectively. Paired *t*-tests further indicated that DOC, $a_g(350)$, $TDLP_9$, and $a_g(350)$: DOC were significantly higher ($p < 0.05$) in the AR than in the MR, but were inconclusive for $TDLP_9$-C ($p = 0.10$).

The spectral slope coefficient $S_{275–295}$ exhibited a nonlinear dependence with salinity, in stark contrast to the lack of dependence exhibited by $S_{350–400}$ (Fig. 2F). The $S_{275–295}$ increased exponentially from a minimum value of 0.0135 nm^{-1} in rivers to a maximum value of 0.0482 nm^{-1} in oligotrophic marine waters. Comparatively, the range of $S_{275–295}$ values in the AR and MR (0.0135–0.0169 nm^{-1}) was minimal. Furthermore, $S_{275–295}$ averaged 0.0156 nm^{-1} in the MR and 0.0150 nm^{-1} in the AR, and a paired *t*-test indicated these values were not significantly different ($p = 0.09$). The dependence of $S_{275–295}$ with salinity also exhibited low seasonal variability with the exception of the summer, when $S_{275–295}$ in the MR, AR, and ocean was noticeably higher. A careful examination of each $a_g(\lambda)$ spectrum demonstrated that the lack of coherent trend for $S_{350–400}$ is not attributable to sensitivity issues with the spectrophotometer. Note, however, that the $S_{350–400}$ of 9 samples (out of 222) were not shown in Fig. 2F because the detection limit of the spectrophotometer was reached at $\lambda < 400$ nm for these samples.

Relationships between optical properties and chemical composition of DOM—A positive, linear relationship ($R^2 \simeq 0.93$) was observed between $TDLP_9$ and $a_g(350)$ (Fig. 3A). This relationship held for all seasons ($0.89 < R^2 < 0.99$), but a seasonality in the lignin contribution to

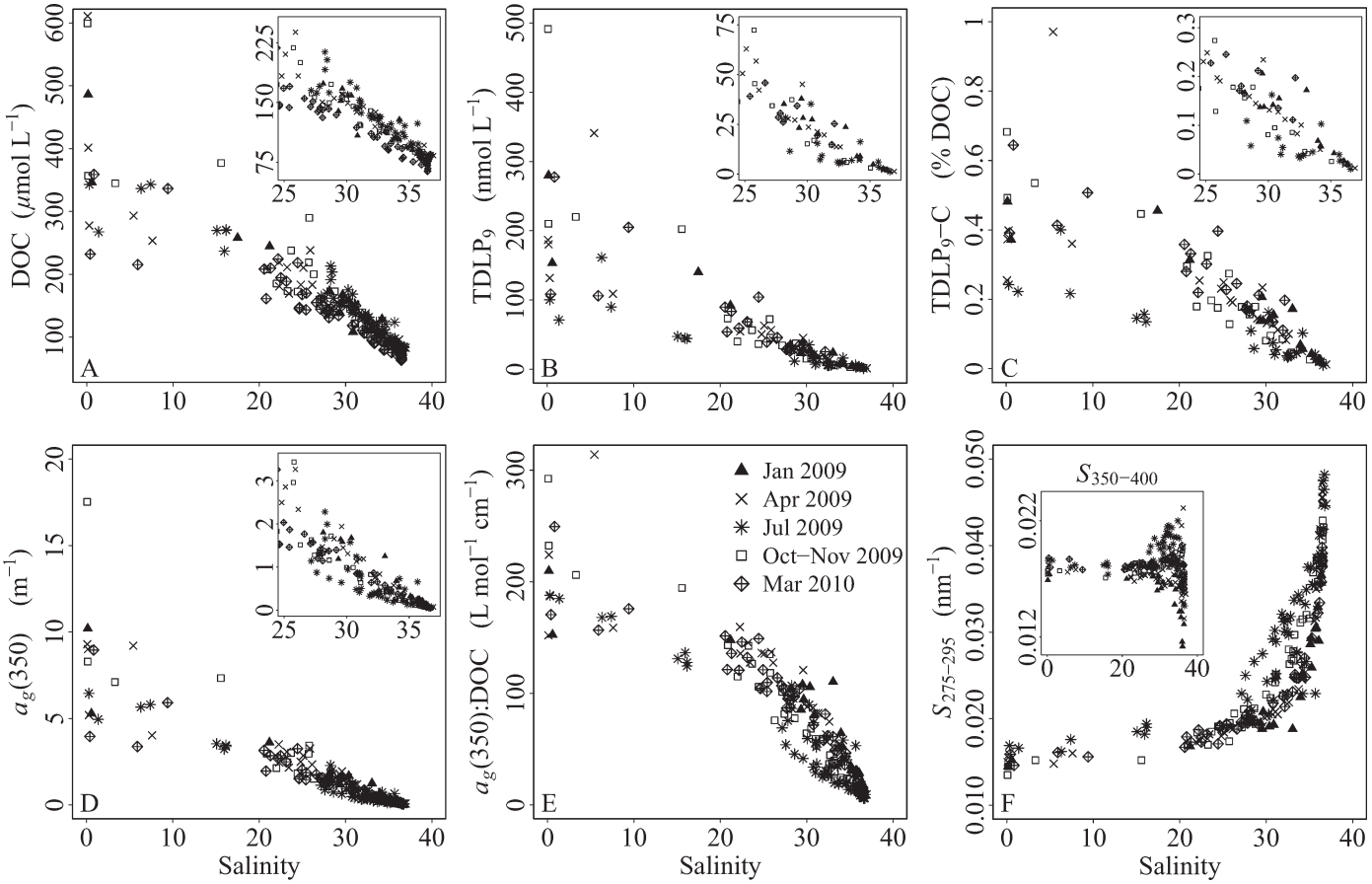

Fig. 2. Relationships between salinity and (A) DOC, (B) $TDLP_9$, (C) $TDLP_9$-C, (D) $a_g(350)$, (E) $a_g(350):DOC$, and (F) $S_{275–295}$ in the NGoM. (A–D) The inset plots provide enhanced views of the relationships at salinities > 25. (F) The inset demonstrates the lack of dependence of $S_{350–400}$ on salinity.

CDOM is evident from seasonal differences in the value of slope coefficient b of Eq. $TDLP_9 = a + b\, a_g(350)$. Minimum and maximum contributions were observed in summer 2009 ($b = 14.8$) and spring 2010 ($b = 32.9$), respectively. This strong linear relationship also implies that $a_g(350)$ can be used as a reliable indicator of $TDLP_9$. A simple model based on Eq. 2 was developed,

$$\ln[\mathrm{TDLP_9}] = \alpha + \beta \ln\left[a_g(350)\right] \tag{2}$$

where the regression parameters α and β are provided in Table 2. The linear regression utilized log-linearized values because both $a_g(350)$ and $TDLP_9$ varied by more than two orders of magnitude. An error analysis revealed that $TDLP_9$ is estimated from $a_g(350)$ within $\pm$ 22% using this simple model.

A striking relationship between $S_{275–295}$ and $a_g(350):DOC$ demonstrated that $S_{275–295}$ is an excellent indicator of the DOC-normalized absorption coefficient in this environment (Fig. 3B). Low values of $S_{275–295}$ are indicative of high DOC-normalized absorption coefficients in rivers, whereas high values of $S_{275–295}$ correspond to low DOC-normalized absorption coefficients in marine waters. No seasonality was observed. A simple model based on Eq. 3 can be used to derive $a_g(350):DOC$ from $S_{275–295}$ in the NGoM,

$$a_g(350):\mathrm{DOC} = e^{(\alpha - \beta S_{275-295})} + e^{(\gamma - \delta S_{275-295})} \tag{3}$$

where the regression coefficients α, β, γ, and δ are provided in Table 2. An error analysis indicated $a_g(350):DOC$ is retrieved from $S_{275–295}$ within $\pm$ 8%.

Finally, a nonlinear relationship between $S_{275–295}$ and $TDLP_9$-C was observed (Fig. 4A). Low values of $S_{275–295}$ were indicative of high $TDLP_9$-C in rivers, whereas high values of $S_{275–295}$ corresponded to low $TDLP_9$-C in marine waters. No seasonality was evident. The nonlinear regression of $TDLP_9$-C on $S_{275–295}$ with Eq. 4 provided the best fit over the entire range of $TDLP_9$-C values (Fig. 4A),

$$\mathrm{TDLP_9\text{-}C} = e^{(\alpha + \beta S_{275-295})} + e^{(\gamma S_{275-295})} + \delta e^{S_{275-295}} \tag{4}$$

where α, β, γ, and δ are the regression coefficients provided in Table 2. The nonlinear regression was weighted with a $1:TDLP_9$-C function for a balanced fit and a more representative model at low $TDLP_9$-C values. A comparison of measured and estimated $TDLP_9$-C demonstrated that the model estimated $TDLP_9$-C from $S_{275–295}$ within $\pm$ 16% of measured $TDLP_9$-C values, consistently over the entire range of $TDLP_9$-C values (Fig. 4B). The error distribution was approximately normal and centered on

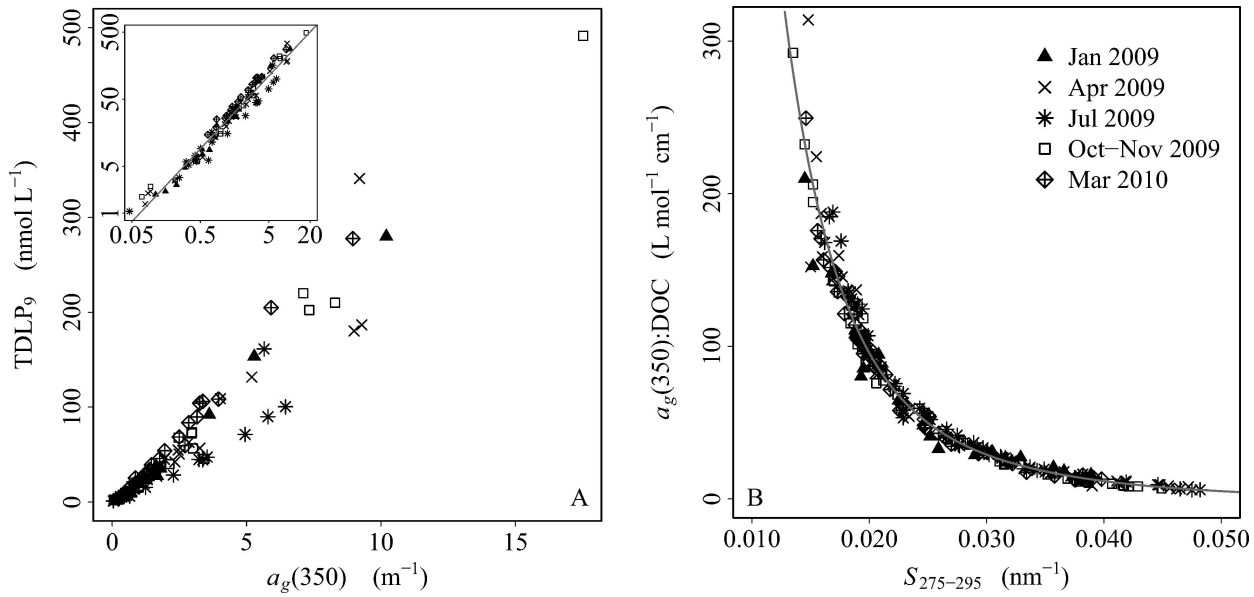

Fig. 3. Relationship between (A) $TDLP_9$ and $a_g(350)$, and (B) $a_g(350):DOC$ and $S_{275–295}$. (A) The inset shows $TDLP_9$ vs. $a_g(350)$ on a log–log scale and the gray fitted line is defined by Eq. 2 and the corresponding coefficients (Table 2). (B) The gray fitted curve is defined by Eq. 3 and the corresponding coefficients are shown in Table 2.

zero with half of the estimates within ± 10% error (boxplot in Fig. 4B). A strong linear relationship ($R^2 \simeq 0.83$) between $S_{275–295}$ and $TDLP_9$-C was also observed for the AR and MR samples alone ($n = 10$).

Models based on the relationships between $a_g(350)$ and $TDLP_6$ (as in Eq. 2), and between $S_{275–295}$ and $TDLP_6$-C (as in Eq. 4) were also derived because the sum of six vanillyl and syringyl lignin phenols is commonly reported in the literature. Excellent linear relationships between $TDLP_6$ and $TDLP_9$ ($R^2 \simeq 0.999$), and between $TDLP_6$-C and $TDLP_9$-C ($R^2 \simeq 0.999$), justified the simple reparameterization of Eq. 2 ($TDLP_6$) and Eq. 4 ($TDLP_6$-C) to derive the models. Their accuracy was slightly less than for $TDLP_9$ and $TDLP_9$-C, thereby supporting the primary use of $TDLP_9$ and $TDLP_9$-C in this study. Regression coefficients and error analyses are provided in Table 2. Note that the parameters and error analyses for all models (Table 2) are only adequate for the range of data collected in this study, and the reliability of the models cannot be guaranteed beyond the range of these variables: $a_g(350)$ (0.046–17.52 m^{-1}), $a_g(350):DOC$ (6–292 L mol^{-1} cm^{-1}), and $S_{275–295}$ (0.0135–0.0482 nm^{-1}).

Experimental results—The riverine DOM mixing experiment demonstrated that $S_{275–295}$ is a conservative tracer of $TDLP_9$-C during mixing (Fig. 5). Salinity and pH increased from 0 and 7.4 respectively in the riverine end member (E0), to 36.6 and 8.1 in the marine end member (F5), which is representative of the salinity and pH ranges typically observed in the NGoM. The $S_{275–295}$ measured in the mixed solutions remained very close to the theoretical $S_{275–295}$ values calculated from mixing ratios and end-member values. The $S_{275–295}$ remains essentially unaffected by changes in the chemical environment of DOM (e.g., pH, ionic strength) during the mixing of river water in the ocean.

Photochemical experiments with 75 samples from the NGoM revealed that exposure of DOM to solar radiation consistently increased $S_{275–295}$ (Fig. 6A). Regardless of season, origin of sample, and irradiation time, $a_g(\lambda)$ always decreased and $S_{275–295}$ always increased during irradiation. The increasingly steeper lines with decreasing $a_g(350)$ (Fig. 6A) further indicated that the rate of change in $S_{275–295}$ relative to that of $a_g(350)$ is lowest in rivers and increases exponentially in the most oligotrophic marine waters (e.g., lowest $a_g[350]$). In contrast, the effects of

Table 2. Coefficients and uncertainties associated with models developed for the retrieval of $TDLP_9$ or $TDLP_6$ from $a_g(350)$ (Eq. 2), and for the estimation of $a_g(350):DOC$ and $TDLP_9$-C or $TDLP_6$-C from $S_{275–295}$ (Eqs. 3 and 4, respectively).

Model	Output	Input	Coefficients				Uncertainty in estimates
			α	β	γ	δ	
Eq. 2	$TDLP_9$	$a_g(350)$	2.966	1.088	—	—	±22%
Eq. 2	$TDLP_6$	$a_g(350)$	2.525	1.263	—	—	±25%
Eq. 3	$a_g(350):DOC$	$S_{275–295}$	5.679	81.229	8.459	241.052	±8%
Eq. 4	$TDLP_9$-C	$S_{275–295}$	3.172	−267.566	0.228	−0.953	±16%
Eq. 4	$TDLP_6$-C	$S_{275–295}$	3.100	−273.952	0.387	−0.969	±20%

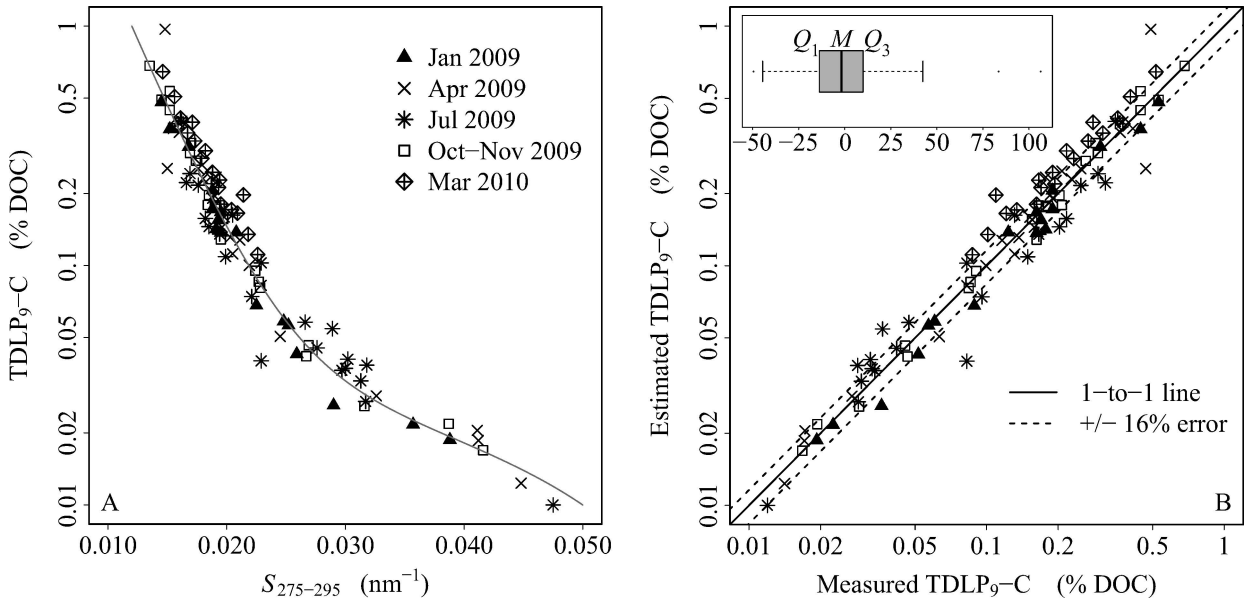

Fig. 4. (A) Relationship between $TDLP_9$-C and $S_{275–295}$ and nonlinear regression curve of $TDLP_9$-C on $S_{275–295}$ (gray curve) defined by Eq. 4 and the corresponding coefficients (Table 2). (B) Plot of $TDLP_9$-C values estimated from $S_{275–295}$ against measured $TDLP_9$-C values. The inset boxplot represents the distribution of error (%) associated with estimated $TDLP_9$-C values relative to measured $TDLP_9$-C values: M = median, Q_1 = first quartile, Q_3 = third quartile, and whiskers are set at ± 1.5× the interquartile range. $TDLP_9$-C can be estimated from $S_{275–295}$ within ± 16% in the NGoM and the error is consistent over the entire range of $TDLP_9$-C values.

photobleaching were highly unpredictable for $S_{350–400}$ and other SSCs estimated in the UV-A and visible regions (e.g., $S_{300–400}$, $S_{300–350}$), varying greatly in direction and magnitude depending on sample origin or irradiation time, but without any clearly discernible pattern. A careful examination of the $a_g(\lambda)$ spectra demonstrated that the unpredictable effects of photodegradation on $S_{350–400}$ are not related to sensitivity issues with the spectrophotometer.

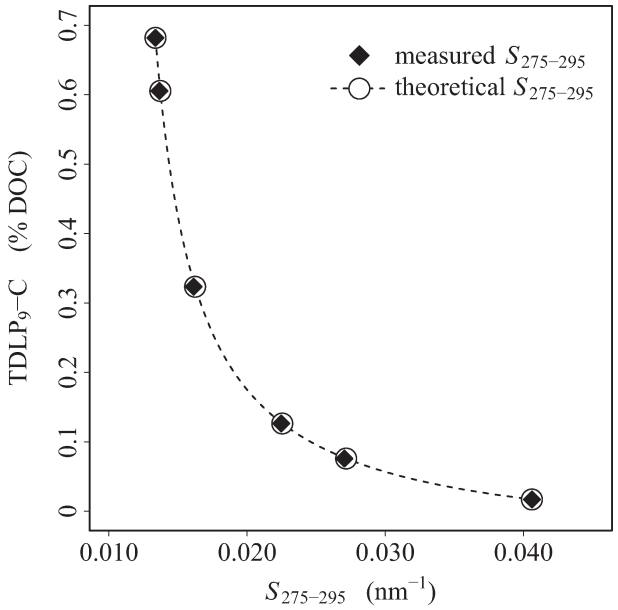

Fig. 5. Riverine DOM mixing experiment used to assess the potential of measured $S_{275–295}$ to trace $TDLP_9$-C during a simple mixing event.

This unpredictability is also evident in the data presented in tables 2 and 3 of Helms et al. (2008). The lignin photodegradation experiments further revealed that increases in $S_{275–295}$ during irradiation were accompanied by decreases in $TDLP_9$-C in all five samples (Fig. 6B).

The DOM amendment and degradation experiments demonstrated that plankton CDOM production had moderate effects on $S_{275–295}$ (Table 3). The addition of ≃ 22 μmol DOC L^{-1} plankton DOM increased $S_{275–295}$ from 0.0168 nm^{-1} to 0.0176 nm^{-1} in sample A1 and from 0.0196 nm^{-1} to 0.0204 nm^{-1} in sample C1. This increase in $S_{275–295}$ is consistent with the measured $S_{275–295}$ (0.0259 nm^{-1}) in the plankton DOM inoculum. HPLC measurements further revealed that total hydrolyzable dissolved amino acids (TDAA) comprise ≃ 20% of DOC in the plankton DOM inoculum. The plankton DOM addition resulted in a 260% and 290% increase in TDAA in samples A1 and C1, respectively. Proteins typically exhibit broad absorption bands centered at 280 nm (Creighton 1993). The large increase in TDAA resulting from the addition of protein-rich plankton DOM is consistent with the observed increase in $S_{275–295}$. This indicates that the production of protein-rich plankton DOM can affect $S_{275–295}$.

The DOM amendment and degradation experiments further revealed that microbial degradation had minor effects on $S_{275–295}$ but might play an important role by balancing the effects of plankton DOM production (Table 3). Microbial degradation in the 'no addition' treatments resulted in a 1% decrease in $S_{275–295}$ after a 10-d incubation in sample C1, and a 2.4% decrease after a 12-d incubation in sample A1. The effects of microbial degradation were more substantial in the plankton DOM addition treatments, with $S_{275–295}$ decreasing from

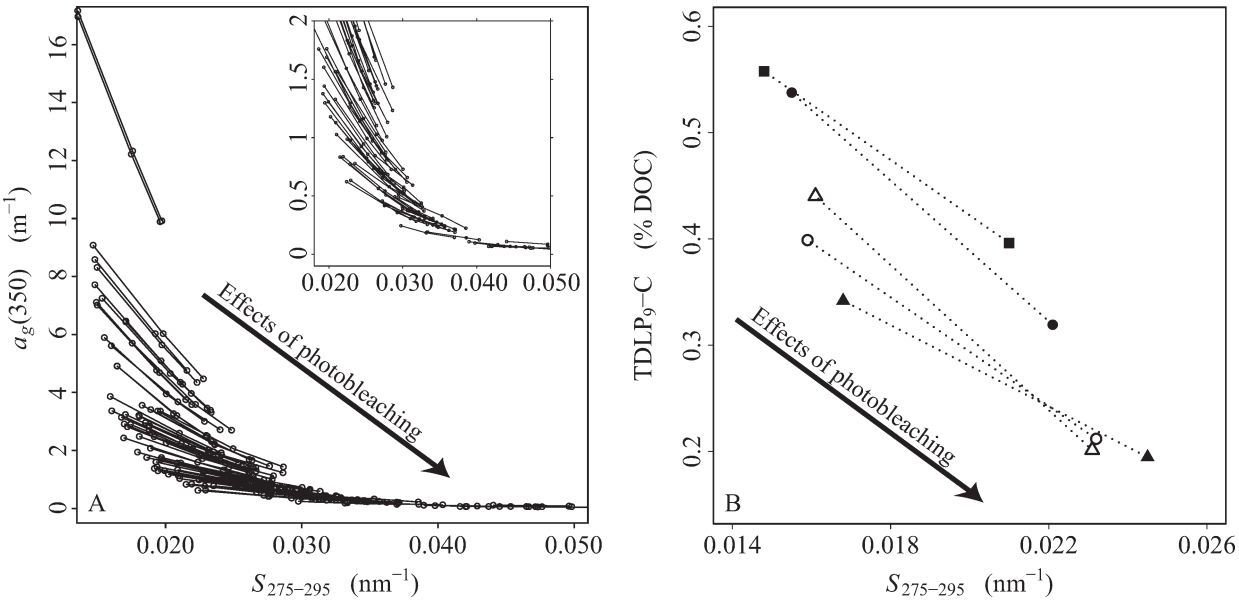

Fig. 6. (A) Changes in $S_{275–295}$ and $a_g(350)$ as a result of photobleaching for 75 samples collected in the NGoM. Each individual line represents a different sample and each circle represents a time point. The inset provides an enhanced view for $a_g(350) \leq 2$ m^{-1}. (B) Changes in TDLP$_9$-C and $S_{275–295}$ upon 48 h irradiation (solar simulator, 750 W) for five samples collected in March 2010 in the Mississippi River plume (open symbols) and in the Atchafalaya River plume (closed symbols). These five samples span a salinity range of 0 to 20.6.

0.0176 nm^{-1} to 0.0165 nm^{-1} in sample A1 and from 0.0204 nm^{-1} to 0.0189 nm^{-1} in sample C1. This enhanced decrease in $S_{275–295}$ to below pre-addition values was also accompanied by a large decrease in DOC and TDAA to pre-addition levels, thereby revealing that most of the plankton DOC added to samples C1 and A1 was remineralized within 10–12 d of incubation. The rapid removal of added DOM is consistent with plankton DOM being primarily composed of labile DOM such as proteins, and demonstrates that microbial degradation has the potential to rapidly neutralize the effects of plankton DOM additions on $S_{275–295}$.

$S_{275–295}$ as a tracer of tDOC—The relationship between $S_{275–295}$ and TDLP$_9$-C can be used to develop the $S_{275–295}$ as a tracer of tDOC in the NGoM (Fig. 7). Lignin is a biomarker of terrigenous DOC, and TDLP$_9$-C can be used to estimate the fraction of terrigenous DOC (%tDOC) in the ocean (Meyers-Schulte and Hedges 1986; Opsahl and Benner 1997; Benner et al. 2005). The %tDOC was calculated as in Eq. 5

$$\%\text{tDOC} = 100\left(\text{TDLP}_9\text{-C}_{\text{sample}}\right)\left(\text{TDLP}_9\text{-C}_{\text{river}}\right)^{-1} \quad (5)$$

where TDLP$_9$-C$_{\text{sample}}$ and TDLP$_9$-C$_{\text{river}}$ are the percentages of DOC comprised by lignin in samples and rivers, respectively. Here, TDLP$_9$-C$_{\text{sample}}$ was estimated from $S_{275–295}$ using Eq. 4, and TDLP$_9$-C$_{\text{river}}$ was calculated as the average of all TDLP$_9$-C values measured in the MR

Table 3. Results from DOM amendment and microbial degradation experiments. Incubation time was 12 d for Sta. A1 and 10 d for Sta. C1.

	Unamended		Plankton DOM addition	
	t=0	t=final	t=0	t=final
Station A1: Off Mobile Bay, Alabama (salinity=23.3)				
DOC (μmol L^{-1})	168.0±1.1	157.8±0.8	190.8±0.6	159.6±1.1
TDAA (nmol L^{-1})	897.0±11.4	643.3±14.1	2331.0±18.0	948.6±11.5
$a_g(350)$ (m^{-1})	2.35	2.36	2.55	2.34
$S_{275–295}$ (nm^{-1})	0.0168	0.0164	0.0176	0.0165
Station C1: Off Terrebonne Bay, Louisiana (salinity=27.8)				
DOC (μmol L^{-1})	133.6±0.7	132.1±1.1	157.5±0.5	130.0±1.1
TDAA (nmol L^{-1})	730.9±34.9	670.3±35.5	2141.7±49.6	858.9±11.1
$a_g(350)$ (m^{-1})	1.25	1.19	1.42	1.35
$S_{275–295}$ (nm^{-1})	0.0196	0.0194	0.0204	0.0189

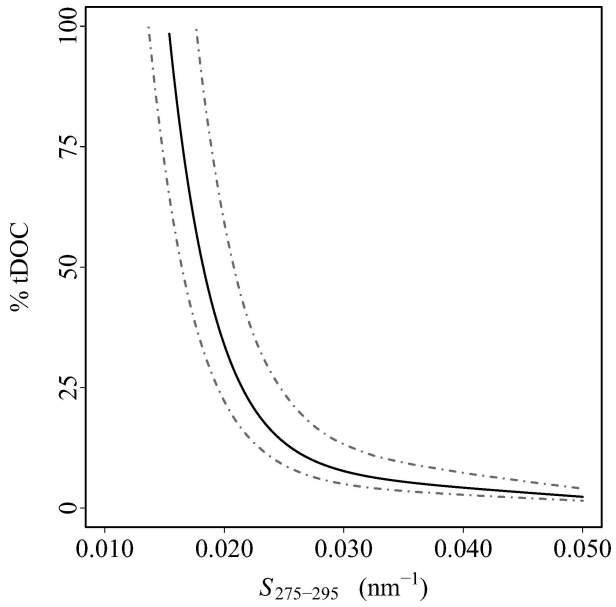

Fig. 7. $S_{275–295}$ as an indicator of %tDOC, the fraction of DOC of terrigenous origin. The values on the solid curve were calculated with Eq. 5, where $TDLP_9\text{-}C_{sample}$ was estimated from $S_{275–295}$ using Eq. 4 and the coefficients of Table 2, and the value $TDLP_9\text{-}C_{river}$ = 0.43 %DOC. The dashed curves delineate the 75% confidence interval of predicted %tDOC calculated using an uncertainty analysis based on the known uncertainties in $TDLP_9\text{-}C_{sample}$ and $TDLP_9\text{-}C_{river}$.

and AR. The error associated with the retrieval of $TDLP_9\text{-}C_{sample}$ from $S_{275–295}$ and the uncertainty in $TDLP_9\text{-}C_{river}$ set limits on the accuracy of the tracer. It was demonstrated earlier that $TDLP_9$-C is retrieved from $S_{275–295}$ with an average error of ± 16%. The uncertainty in $TDLP_9\text{-}C_{river}$, on the other hand, is related to the natural variability of $TDLP_9$-C in the MR and AR, where it averaged 0.38 ± 0.10 %DOC (range = 0.22–0.49) and 0.48 ± 0.2 %DOC (range = 0.24–0.68), respectively. Considering that tDOC and lignin in NGoM surface waters primarily originate from the MR and AR, $TDLP_9\text{-}C_{river}$ in surface waters of the NGoM is best represented by a normal distribution with mean 0.43 %DOC and standard deviation 0.15 %DOC, corresponding to the mean and standard deviation of all $TDLP_9$-C measurements made in the AR and MR (n = 10). An uncertainty analysis based on the consideration of these two sources of error was performed and a 75% confidence interval of predicted %tDOC was calculated (Fig. 7). The approach can also be applied using $TDLP_6\text{-}C_{sample}$ and $TDLP_6\text{-}C_{river}$, where $TDLP_6\text{-}C_{river}$ in surface waters of the NGoM is best represented by a normal distribution with mean 0.35 %DOC and standard deviation 0.13 %DOC.

Discussion

The applicability of the tDOC tracer presented in this manuscript relies on the existence of a strong relationship between $S_{275–295}$ and $TDLP_9$-C, which arises primarily from a combination of the following factors: (1) lignin is a chromophore unique to DOC of terrestrial origin; (2) photodegradation of CDOM consistently leads to an increase in $S_{275–295}$ and a decrease in $TDLP_9$-C; and (3) mixing and photobleaching are dominant processes regulating $S_{275–295}$ and $TDLP_9$-C in surface waters of river-influenced ocean margins.

Response of $S_{275–295}$ *to photobleaching*—Although spectral features of CDOM absorption have long been recognized as potentially informative in the characterization of DOM (Carder et al. 1989; Chin et al. 1994; Peuravuori and Pihlaja 1997), variability in SSCs in the marine environment have proven difficult to interpret. The lack of clear trends in the ocean and the inconsistent spectral range and methodology used in the derivation of the SSC are primarily responsible for the lack of consensus on the use of this parameter in the marine environment (Blough and Del Vecchio 2002). The value of the SSC depends on the spectral range considered, thereby reflecting the inadequacy of the single exponential model (Eq. 1) to capture the spectral nuances exhibited by $a_g(\lambda)$ (Twardowski et al. 2004). A single exponential model only provides a reasonable description of the spectrum over narrow spectral regions. These limitations led Helms et al. (2008) to propose the use of narrow SSCs as biogeochemical indicators. They demonstrated that $S_{275–295}$ and the dimensionless slope ratio S_R ($S_{275–295}$: $S_{350–400}$) were strongly related to CDOM average molecular weight. They further revealed that $S_{275–295}$ and S_R consistently increased upon irradiation and suggested they are potential indicators of photobleaching in the marine environment. An increase in $S_{275–295}$ upon irradiation of water samples from the Southern Ocean (Ortega-Retuerta et al. 2009) and the Congo River (first 12 d of irradiation; Spencer et al. 2009) has been observed and is consistent with the data presented herein.

The present study also revealed that the response of $S_{275–295}$ to irradiation is unique among SSCs. The effects of irradiation were more pronounced for $S_{275–295}$ than for spectrally adjacent SSCs (e.g., $S_{254–275}$, $S_{295–320}$) and lead to unpredictable effects for SSCs with $\lambda > 320$ nm (e.g., $S_{350–400}$). In general, the net effects of photobleaching on SSCs are highly dependent on the spectral quality of irradiation (Tzortziou et al. 2007) and are therefore sensitive to spectral variations in incident solar irradiance, water column diffuse attenuation, and $a_g(\lambda)$ in the marine environment. In contrast to other SSCs, the response of $S_{275–295}$ to solar irradiation is unique because of the position of the 275–295-nm window on the outer edge of the incident solar spectrum. Few photons of wavelength < 295 nm are present in the environment, and under almost all natural aquatic conditions the rate of photon absorption by CDOM decreases sharply from 295 nm to 275 nm. Furthermore, the extensive work of Del Vecchio and Blough (2002, 2004*b*) on photobleaching indicates the fraction of initial $a_g(\lambda)$ lost upon absorption of photons ≥ 295 nm is always greater at 295 nm than at 275 nm. Consequently, exposure of CDOM to solar radiation under natural conditions always results in a greater fractional decrease in $a_g(295)$ than in $a_g(275)$, thereby increasing $S_{275–295}$. This unique feature of $S_{275–295}$ makes it an

excellent indicator of photobleaching and is critical for its application as a proxy of $TDLP_9$-C in river-influenced ocean margins.

Dynamics and regulatory processes of $S_{275–295}$—The inflow of riverine inputs from the MR and AR and its physical mixing on the shelf represents a dominant mechanism regulating the dynamics of $S_{275–295}$ in the surface waters of the NGoM. The prominent role of riverine inputs on CDOM in the NGoM was revealed in previous studies (Chen et al. 2004; D'Sa and DiMarco 2009) and is confirmed here by the linearity of the seasonal trends in $a_g(350)$ and $TDLP_9$ with salinity. The observation that the exponential dependence of $S_{275–295}$ on salinity closely resembles a conservative SSC mixing curve (Stedmon et al. 2003) demonstrates the importance of mixing in the regulation of $S_{275–295}$ across the entire salinity gradient. The dynamics of $S_{275–295}$ are sensitive to variations in $S_{275–295}$ in the MR and AR, but the narrow range of $S_{275–295}$ values in the MR and AR (0.0135–0.0169 nm^{-1}) relative to that observed along the salinity gradient (0.0135–0.0482 nm^{-1}) indicates that the natural variability of $S_{275–295}$ in the MR and AR represents a minor driver of the variability in the NGoM. These effects were most noticeable during the summer.

The large range of $S_{275–295}$ values along the salinity gradient indicates the influence of other regulatory processes. The riverine DOM mixing experiment revealed minimal effects of pH and ionic strength on $S_{275–295}$ and is in agreement with the findings of Blough et al. (1993) and Guo et al. (2007) in other river-influenced systems. A simple sensitivity analysis using measured nitrate and nitrite concentrations on 217 of the 222 samples used in this study and the published molar absorption coefficients of aqueous nitrate and nitrite (Gaffney et al. 1992; Riordan et al. 2005) demonstrated that these inorganic species contribute minimally to the variability of $S_{275–295}$ in the NGoM. Biological processes also appeared to play a minor role in the regulation of $S_{275–295}$ because microbial degradation resulted in lower $S_{275–295}$ values, as was observed by Helms et al. (2008) and Ortega-Retuerta et al. (2009), and plankton-derived DOC and CDOM were rapidly consumed by microorganisms. Thus, neither biological processes nor changes in pH, ionic strength, nitrate, or nitrite can account for the observed dynamics and trends in $S_{275–295}$.

This study demonstrated that photobleaching is a major process regulating $S_{275–295}$ in surface waters. During transport from rivers to the outer shelf, CDOM mixes with waters of varying optical properties and is exposed to changing irradiation conditions. In light of the contrasting responses of $S_{275–295}$ and $S_{350–400}$ to solar exposure demonstrated in this study, the monotonic increase in $S_{275–295}$ with salinity and the corresponding lack of a coherent trend in $S_{350–400}$ are both consistent with the cumulative effects of photobleaching on CDOM. Furthermore, the observation that $S_{275–295}$ exhibits a greater range of values than other SSCs in the NGoM is also consistent with the prominent regulatory role of photobleaching and the greater sensitivity of $S_{275–295}$ to photobleaching relative to other SSCs. Higher $S_{275–295}$ values observed at salinities > 25 during summer are consistent with the enhancement of photobleaching by high solar irradiance and shallow stratification of surface waters on the shelf. The strong relationship between $S_{275–295}$ and $a_g(350)$: DOC is consistent with evidence that photobleaching also decreases $a_g(\lambda)$: DOC very efficiently (Stubbins et al. 2010).

$S_{275–295}$*, CDOM MW, and lignin MW*—The large increase in $S_{275–295}$ along the salinity gradient is evidence that the suite of chromophores in riverine and marine CDOM is very different. A simple decrease in the abundance of chromophores with increasing salinity would result in a decrease in $a_g(\lambda)$ but would leave $S_{275–295}$ unchanged, as a simple dilution of river water in milli-Q water can demonstrate. Chromophoric compounds can vary because they originate from different sources (terrigenous vs. marine), as revealed by the large difference in $S_{275–295}$ between rivers (0.0135–0.0169 nm^{-1}) and fresh plankton DOM (0.0259 nm^{-1}) observed in this study. Chromophores can also change as a result of photochemical or biological transformations in the water column. However, as previously discussed, photochemical degradation stands alone as a process capable of producing $S_{275–295}$ values > 0.03 nm^{-1}, thereby suggesting that CDOM is photo-chemically altered in surface waters of salinities > 30, regardless of origin (i.e., marine or terrigenous).

The results of this study are consistent with $S_{275–295}$ being closely related to CDOM MW in the NGoM (Helms et al. 2008). Biological processing, nitrate and nitrite concentrations, and CDOM alterations resulting from changes in pH and ionic strength have minimal effects on $S_{275–295}$. In contrast, the mixing of different chromophores and the cumulative effects of photobleaching appear largely responsible for the increasing trend in $S_{275–295}$ with salinity. Solar exposure is known to decrease CDOM MW (Mopper and Kieber 2002). Benner and Opsahl (2001) demonstrated that the MW of DOC decreases across salinity gradients in the NGoM, and Helms et al. (2008) revealed that $S_{275–295}$ consistently increases with photo-chemically induced decreases in MW for a wide range of natural waters. Thus, the increase in $S_{275–295}$ with salinity observed in the NGoM is most likely representative of a decrease in CDOM MW along the salinity gradient. Consistent with this idea, continuous shifts from high MW to low MW CDOM along the freshwater–marine continuum were reported in the lower Chesapeake Bay (Helms et al. 2008) and in the St.-Lawrence Estuary (Xie et al. 2012).

It appears $S_{275–295}$ is also related to lignin MW in the NGoM. Lignin is an aromatic heteropolymer and a known chromophore. Lignin concentrations co-vary strongly with $a_g(350)$ across the MR plume (Hernes and Benner 2003) and in the Yukon River basin (Spencer et al. 2008). Furthermore, the present study revealed that a strong relationship exists between $a_g(350)$ and lignin concentration throughout surface waters of the NGoM during all seasons, thereby indicating that lignin in this environment is primarily regulated by the same dominant mechanisms as the rest of CDOM. Solar exposure of CDOM results in a

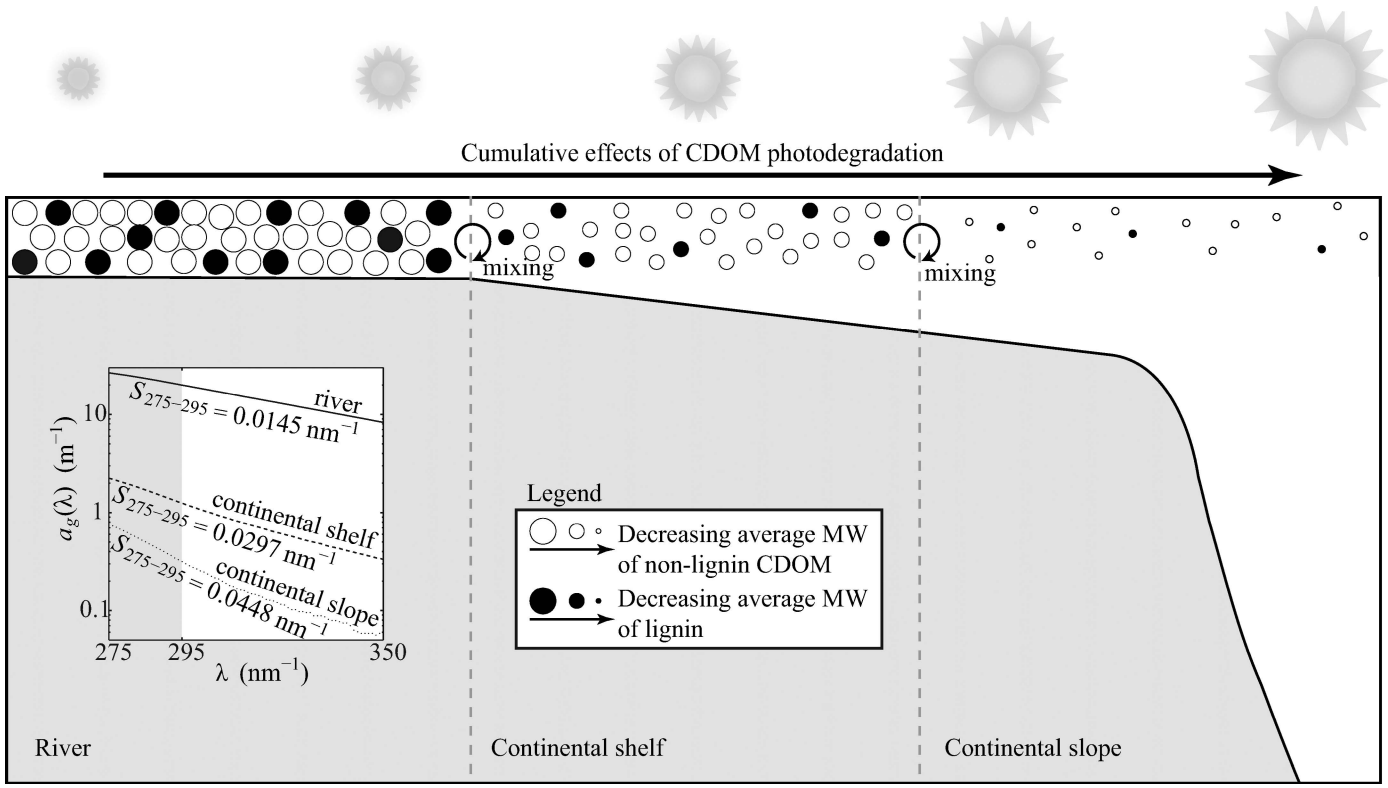

Fig. 8. Conceptual illustration of the relationship between $S_{275–295}$ and TDLP$_9$-C. The value of $S_{275–295}$ is closely linked to the average MW of CDOM and lignin. On the continental shelf and slope of the NGoM, mixing and photodegradation are major processes controlling the lignin content of DOC and the MW distribution of lignin and other chromophores in surface waters. These processes shape the relationship between $S_{275–295}$ and TDLP$_9$-C along the river-to-ocean waters continuum.

simultaneous decrease in lignin concentration and $a_g(350)$ (Spencer et al. 2009; Benner and Kaiser 2011) and therefore tends, like mixing, to preserve the relationship between lignin concentration and $a_g(350)$. Opsahl and Benner (1998) observed a shift in lignin MW from 90% high MW to 80% low MW upon 28 d of incubation in sunlight, and alteration of lignin composition further indicates that solar exposure is responsible for the sharp decrease in lignin MW observed along the salinity gradient of the MR plume (Benner and Opsahl 2001; Hernes and Benner 2003). These observations suggest $S_{275–295}$ is tightly linked to lignin MW. Consistent with this idea, recent work on the structural basis of CDOM optical properties suggests that intramolecular interactions between (partially oxidized) lignin aromatic moeities play an important role in determining CDOM absorption properties (Del Vecchio and Blough 2004*a;* Boyle et al. 2009).

$S_{275–295}$ as an indicator of TDLP$_9$-C and as a tracer of terrigenous DOC—The relationship observed between $S_{275–295}$ and TDLP$_9$-C in surface waters of the NGoM arises primarily as a result of the concurrent effects of mixing and photodegradation on the lignin content of DOC and the MW distribution of lignin and other chromophores (Fig. 8). This study revealed that several factors contribute to maintaining the relationship between $S_{275–295}$ and TDLP$_9$-C throughout the river-to-ocean continuum in the NGoM. First, $S_{275–295}$ and TDLP$_9$-C are strongly and linearly correlated in the MR and AR and exhibit little variability in these rivers relative to their range of variability in the marine environment. A strong relationship between comparable properties (lignin yield and slope ratio, S_R), was also observed in the upland catchments of the Congo River (Spencer et al. 2010). Second, $S_{275–295}$ is a conservative tracer of TDLP$_9$-C during mixing of freshwater in the ocean. Third, photodegradation of CDOM consistently increases $S_{275–295}$ while decreasing TDLP$_9$-C, thereby indicating that photodegradation results in the simultaneous decrease in CDOM and lignin MW and the removal of lignin from the DOC pool. Finally, microbial degradation shows little potential for altering TDLP$_9$-C on time scales of ocean-margin dynamics (Opsahl and Benner 1998; Hernes and Benner 2003). The elevated production of marine DOC by planktonic organisms often observed at salinities of 20–30 (Benner and Opsahl 2001) tends to disrupt this relationship and might be responsible for the increased scatter in data corresponding to these salinities.

The dual nature of lignin as a chromophore and a terrigenous component of DOC enables the use of $S_{275–295}$ as a tracer of the fraction of tDOC in a water sample, thereby providing new capabilities to trace tDOC on synoptic scales of significance to carbon cycling in ocean

margins. It is important to note, however, that quantitative applications of this tracer assume that preferential removal of lignin from tDOC by photochemical processes is balanced by preferential removal of other components of tDOC by microbial processes on times scales of ocean-margin dynamics. Although further studies of the relative kinetics of these processes in surface waters of river-influenced ocean margins is required to assess the extent to which this tracer is representative of bulk tDOC, the observation that photodegradation and biodegradation preferentially remove distinct components of riverine DOM on ocean-margin time scales provides support for this assumption (Benner and Kaiser 2011). Based on this assumption, Eqs. 4 and 5 can be used to estimate the %tDOC from optical measurements of $S_{275–295}$ in river-influenced ocean margins. In light of the recent work of Fichot and Benner (2011), this tracer provides new capabilities to estimate the concentration of tDOC and marine DOC from optical measurements of $a_g(\lambda)$ in the 275–295-nm range.

The application of this tracer is constrained to marine environments where a relationship between $S_{275–295}$ and $TDLP_9$-C exists. Until its range of applicability is better understood, the use of the tracer should be restricted to surface waters of river-influenced ocean margins where mixing and photobleaching are important processes regulating $S_{275–295}$ and the lignin content of DOC, and where lignin is an important chromophore in the CDOM pool. Because the extent to which photobleaching affects $S_{275–295}$ and $TDLP_9$-C relative to mixing is expected to vary among ocean margins, the parameters of Eq. 4 derived in the NGoM are not expected to apply to all river-influenced ocean margins. Preliminary results suggest that the tracer can be applied to the region of the Southeastern Beaufort Sea (Arctic Ocean) influenced by the Mackenzie River after reparameterization of the relationship between $S_{275–295}$ and $TDLP_9$-C. Moreover, the value of $TDLP_9\text{-}C_{river}$ varies among river systems and seasons such that adequate knowledge of the variability in $TDLP_9\text{-}C_{river}$ is required for proper application of the tracer. Because of its practicality and general applicability to river-influenced regions of the ocean, this optical tracer of tDOC represents an important new tool for improving coastal carbon budgets on scales of global significance.

Acknowledgments

We are grateful to Steven E. Lohrenz, Wei-Jun Cai, and Kjell Gundersen for providing berths on the GulfCarbon cruises, and to Leanne Powers and the crews of the R/V *Cape Hatteras* and the R/V *Hugh Sharp* for their assistance with sample collection onboard. We also express our gratitude to Karl Kaiser for his general assistance in the laboratory and Yuan Shen for amino acid analyses. We thank Wei-Jun Cai's group (University of Georgia) for pH measurements and Steven E. Lohrenz's group (University of Southern Mississippi) for sharing nitrate and nitrite data. We thank two anonymous reviewers and Peter Hernes for their time and their constructive comments.

Funding for this work was provided by the National Science Foundation (NSF, grants 0850653 and 0713915 to Ronald Benner, 0752254 to Steven E. Lohrenz, and 0752110 to Wei-Jun Cai).

References

Benner, R., and K. Kaiser. 2011. Biological and photochemical transformations of lignin phenols and amino acids in riverine dissolved organic matter. Biogeochemistry **102:** 209–222, doi:10.1007/s10533-010-9435-4

———, P. Louchouarn, and R. M. W. Amon. 2005. Terrigenous dissolved organic matter in the Arctic Ocean and its transport to surface and deep waters of the North Atlantic. Glob. Biogeochem. Cycles **19:** GB2025, doi:10.1029/2004GB002398

———, and S. Opsahl. 2001. Molecular indicators of the sources and transformations of dissolved organic matter in the Mississippi river plume. Org. Geochem. **32:** 597–611, doi:10.1016/S0146-6380(00)00197-2

———, and M. Strom. 1993. A critical evaluation of the analytical blank associated with DOC measurements by high-temperature catalytic oxidation. Mar. Chem. **41:** 153–160, doi:10.1016/0304-4203(93)90113-3

Blough, N. V., and R. Del Vecchio. 2002. Chromophoric DOM in the coastal environment, p. 509–546. *In* D. Hansell and C. A. Carlson [eds.], Biogeochemistry of marine dissolved organic matter. Academic Press.

———, O. C. Zafiriou, O. C., and J. Bonilla. 1993. Optical absorption spectra of water from the Orinoco outflow—terrestrial input of colored organic matter to the Caribbean. J. Geophys. Res. Oceans **98:** 2271–2278, doi:10.1029/92JC02763

Borges, A. V., B. Delille, and M. Frankignoulle. 2005. Budgeting sinks and sources of CO2 in the coastal ocean: Diversity of ecosystems counts. Geophys. Res. Lett. **32:** L14601, doi:10.1029/2005GL023053

Boyle, E. S., N. Guerriero, A. Thiallet, R. D. Vecchio, and N. V. Blough. 2009. Optical properties of humic substances and CDOM: Relation to structure. Environ. Sci. Technol. **43:** 2262–2268, doi:10.1021/es803264g

Cai, W. J., M. H. Dai, and Y. C. Wang. 2006. Air–sea exchange of carbon dioxide in ocean margins: A province-based synthesis. Geophys. Res. Lett. **33:** L12603, doi:10.1029/2006GL026219

Carder, K. L., R. G. Steward, G. R. Harvey, and P. B. Ortner. 1989. Marine humic and fulvic acids—their effects on remote sensing of ocean chlorophyll. Limnol. Oceanogr. **34:** 68–81, doi:10.4319/lo.1989.34.1.0068

Cauwet, G. 2002. DOM in the coastal zone, p. 579–609. *In* D. Hansell and C. A. Carlson [eds.], Biogeochemistry of marine dissolved organic matter. Academic Press.

Chen, R. F., and others. 2004. Chromophoric dissolved organic matter (CDOM) source characterization in the Louisiana Bight. Mar. Chem. **89:** 257–272, doi:10.1016/j.marchem.2004.03.017

———, and G. B. Gardner. 2004. High-resolution measurements of chromophoric dissolved organic matter in the Mississippi and Atchafalaya River plume regions. Mar. Chem. **89:** 103–125, doi:10.1016/j.marchem.2004.02.026

Chin, Y. P., G. Aiken, and E. Oloughlin. 1994. Molecular weight, polydispersity, and spectroscopic properties of aquatic humic substances. Environ. Sci. Technol. **28:** 1853–1858, doi:10.1021/es00060a015

Creighton, T. 1993. Proteins: Structure and molecular properties, 2nd ed. Freeman.

Davis, J., and R. Benner. 2007. Quantitative estimates of labile and semi-labile dissolved organic carbon in the western Arctic Ocean: A molecular approach. Limnol. Oceanogr. **52:** 2434–2444, doi:10.4319/lo.2007.52.6.2434

Del Vecchio, R., and N. V. Blough. 2002. Photobleaching of chromophoric dissolved organic matter in natural waters: Kinetics and modeling. Mar. Chem. **78:** 231–253, doi:10.1016/S0304-4203(02)00036-1

———, and ———. 2004*a*. Spatial and seasonal distribution of chromophoric dissolved organic matter and dissolved organic carbon in the Middle Atlantic Bight. Mar. Chem. **89:** 169–187, doi:10.1016/j.marchem.2004.02.027

———, and ———. 2004*b*. On the origin of the optical properties of humic substances. Environ. Sci. Technol. **38:** 3885–3891, doi:10.1021/es049912h

Druffel, E. R. M., P. M. Williams, J. E. Bauer, and J. R. Ertel. 1992. Cycling of dissolved and particulate organic matter in the open ocean. J. Geophys. Res. **97:** 15639–15659, doi:10.1029/92JC01511

D'sa, E. J., and S. F. Dimarco. 2009. Seasonal variability and controls on chromophoric dissolved organic matter in a large river-dominated coastal margin. Limnol. Oceanogr. **54:** 2233–2242, doi:10.4319/lo.2009.54.6.2233

Fichot, C. G., and R. Benner. 2011. A novel method to estimate DOC concentrations from CDOM absorption coefficients in coastal waters. Geophys. Res. Lett. **38:** L03610, doi:10.1029/2010GL046152

Gaffney, J. S., N. A. Marley, and M. M. Cunningham. 1992. Measurement of the absorption constants for nitrate in water between 270 and 335 nm. Environ. Sci. Technol. **26:** 207–209, doi:10.1021/es00025a027

Gattuso, J-P., M. Frankignoulle, and R. Wollast. 1998. Carbon and carbonate metabolism in coastal aquatic ecosystems. Annu. Rev. Ecol. Syst. **29:** 405–434, doi:10.1146/annurev.ecolsys.29.1.405

Guo, W., C. A. Stedmon, Y. Han, F. Wu, X. Yu, and M. Hu. 2007. The conservative and non-conservative behavior of chromophoric dissolved organic matter in Chinese estuarine waters. Mar. Chem. **107:** 357–366, doi:10.1016/j.marchem.2007.03.006

Hedges, J., R. Keil, and R. Benner. 1997. What happens to terrestrial organic matter in the ocean? Org. Geochem. **27:** 195–212, doi:10.1016/S0146-6380(97)00066-1

———, and D. Mann. 1979. The characterization of plant tissues by their lignin oxidation products. Geochim. Cosmochim. Acta **43:** 1803–1807, doi:10.1016/0016-7037(79)90028-0

Helms, J. R., A. Stubbins, J. D. Ritchie, E. C. Minor, D. J. Kieber, and K. Mopper. 2008. Absorption spectral slopes and slope ratios as indicators of molecular weight, source, and photobleaching of chromophoric dissolved organic matter. Limnol. Oceanogr. **53:** 955–969, doi:10.4319/lo.2008.53.3.0955

Hernes, P. J., and R. Benner. 2003. Photochemical and microbial degradation of dissolved lignin phenols: Implications for the fate of terrigenous dissolved organic matter in marine environments. J. Geophys. Res. **108:** 3291, doi:10.1029/2002JC001421

Hoge, F. E., M. E. Williams, R. N. Swift, J. K. Yungel, and A. Vodacek. 1995. Satellite retrieval of the absorption coefficient of chromophoric dissolved organic matter in continental margins. J. Geophys. Res. Oceans **100:** 24847–24854, doi:10.1029/95JC02561

Johannessen, S. C., and W. L. Miller. 2001. Quantum yield for the photochemical production of dissolved inorganic carbon in seawater. Mar. Chem. **76:** 271–283, doi:10.1016/S0304-4203(01)00067-6

Kaiser, K., and R. Benner. 2012. Characterization of lignin by gas chromatography and mass spectrometry using a simplified CuO oxidation method. Anal. Chem. **84:** 459–464, doi:10.1021/ac202004r

Louchouarn, P., S. Opsahl, and R. Benner. 2000. Isolation and quantification of dissolved lignin from natural waters using solid-phase extraction and GC/MS. Anal. Chem. **72:** 2780–2787, doi:10.1021/ac9912552

Meyers-Schulte, K. J., and J. I. Hedges. 1986. Molecular evidence for a terrestrial component of organic matter dissolved in ocean water. Nature **321:** 61–63, doi:10.1038/321061a0

Mopper, K., and D. J. Kieber. 2002. Photochemistry and cycling of carbon, sulfur, nitrogen and phosphorus, p. 456–509. *In* D. Hansell and C. A. Carlson [eds.], Biogeochemistry of marine dissolved organic matter. Academic Press.

Muller-Karger, F. E., R. Varela, R. Thunell, R. Luerssen, C. Hu, and J. J. Walsh. 2005. The importance of continental margins in the global carbon cycle. Geophys. Res. Lett. **32:** L01602, doi:10.1029/2004GL021346

Opsahl, S., and R. Benner. 1997. Distribution and cycling of terrigenous dissolved organic matter in the ocean. Nature **386:** 480–482, doi:10.1038/386480a0

———, and ———. 1998. Photochemical reactivity of dissolved lignin in river and ocean waters. Limnol. Oceanogr. **43:** 1297–1304, doi:10.4319/lo.1998.43.6.1297

Ortega-Retuerta, E., T. K. Frazer, C. M. Duarte, S. Ruiz-Halpern, A. Tovar-Sanchez, J. M. Arrieta, and I. Reche. 2009. Biogeneration of chromophoric dissolved organic matter by bacteria and krill in the Southern Ocean. Limnol. Oceanogr. **54:** 1941–1950, doi:10.4319/lo.2009.54.6.1941

Peuravuori, J., and K. Pihlaja. 1997. Molecular size distribution and spectroscopic properties of aquatic humic substances. Anal. Chim. Acta **337:** 133–149, doi:10.1016/S0003-2670(96)00412-6

Rabalais, N. N., R. E. Turner, and W. J. Wiseman. 2002. Gulf of Mexico hypoxia, aka "The dead zone". Annu. Rev. Ecol. Syst. **33:** 235–263, doi:10.1146/annurev.ecolsys.33.010802.150513

Riordan, E., N. Minogue, D. Healy, P. O'driscol, and J. R. Sodeau. 2005. Spectroscopic and optimization modeling study of nitrous acid in aqueous solution. J. Phys. Chem. A **109:** 779–786, doi:10.1021/jp040269v

Shen, Y., C. G. Fichot, and R. Benner. 2012. Floodplain influence on dissolved organic matter composition and export from the Mississippi–Atchafalaya River system to the Gulf of Mexico. Limnol. Oceanogr. **57:** 1149–1160, doi:10.4319/lo.2012.57.4.1149

Smith, S. V., and J. T. Hollibaugh. 1993. Coastal metabolism and the oceanic organic carbon balance. Rev. Geophys. **31:** 75–89, doi:10.1029/92RG02584

Spencer, R. G. M., G. R. Aiken, K. P. Wickland, R. G. Striegl, and P. J. Hernes. 2008. Seasonal and spatial variability in dissolved organic matter quantity and composition from the Yukon River basin, Alaska. Glob. Biogeochem. Cycles **22:** GB4002, doi:10.1029/2008GB003231

———, P. J. Hernes, R. Ruf, A. Baker, R. Y. Dyda, A. Stubbins, and J. Six. 2010. Temporal controls on dissolved organic matter and lignin biogeochemistry in a pristine tropical river, Democratic Republic of Congo. J. Geophys. Res. Biogeosciences **115:** G03013, doi:10.1029/2009JG001180

———, and others. 2009. Photochemical degradation of dissolved organic matter and dissolved lignin phenols from the Congo River. J. Geophys. Res. Biogeosciences **114:** G03010, doi:10.1029/2009JG000968

Stedmon, C. A., S. Markager, and R. Bro. 2003. Tracing dissolved organic matter in aquatic environments using a new approach to fluorescence spectroscopy. Mar. Chem. **82:** 239–254, doi:10.1016/S0304-4203(03)00072-0

Stubbins, A., and others. 2010. Illuminated darkness: Molecular signatures of Congo River dissolved organic matter and its photochemical alteration as revealed by ultrahigh precision mass spectrometry. Limnol. Oceanogr. **55:** 1467–1477, doi:10.4319/lo.2010.55.4.1467

Twardowski, M. S., E. Boss, J. M. Sullivan, and P. L. Donaghay. 2004. Modeling the spectral shape of absorption by chromophoric dissolved organic matter. Mar. Chem. **89:** 69–88, doi:10.1016/j.marchem.2004.02.008

Tzortziou, M., C. L. Osburn, and P. J. Neale. 2007. Photobleaching of dissolved organic material from a tidal marsh–estuarine system of the Chesapeake Bay. Photochem. Photobiol. **83:** 782–792, doi:10.1111/j.1751-1097.2007.00142.x

Xie, H., C. Aubry, S. Bélanger, and G. Song. 2012. The dynamics of absorption coefficients of CDOM and particles in the St.-Lawrence estuarine system: Biogeochemical and physical implications. Mar. Chem. **128–129:** 44–56, doi:10.1016/j.marchem.2011.10.001

Associate editor: Peter Hernes

Received: 01 February 2012
Accepted: 22 May 2012
Amended: 05 June 2012